doi:10.3723/ut.36.029 Underwater Technology, Vol. 36, No. 2, pp. 29–35, 2019 www.sut.org

Position estimation for underwater vehicles using unscented Kalman filter with Gaussian process prediction

Wilmer Ariza Ramirez*, Zhi Quan Leong, Hung Nguyen and Shantha Gamini Jayasinghe
University of Tasmania, Australian Maritime College

Received February 2019; Accepted May 2019

Abstract

The present paper explores the use of Gaussian process-unscented Kalman filter (GP-UKF) algorithm for position estimation of underwater vehicles. GP-UKF has a number of advantages over parametric unscented Kalman filters (UKFs) and Bayesian filters, such as improved tracking quality and graceful degradation with the increase of model uncertainty. The advantage of Gaussian process (GP) over parametric models is that GP considers noise and uncertainty in model identification. These qualities are highly desired for underwater vehicles as the number and quality of sensors available for position estimation are limited. The application of non-parametric models on navigation for underwater vehicles can lead to faster deployment of the platform, reduced costs and better performance than parametric methodologies. In the present study, a REMUS 100 parametric model was employed for the generation of data and internal model in the calculation to compare the performance of an ideal UKF against GP-UKF for position estimation. GP-UKF demonstrated better performance and robustness in the estimation of vehicle position and state correction compared to the ideal UKF.

Keywords: Unscented Kalman filter, GP-UKF, Gaussian process, underwater vehicles

Acronymn list:

ADCP	acoustic doppler current profiler
AUV	autonomous underwater vehicles
CFD	computational fluid dynamics
DVL	doppler velocity log
DVS	doppler velocity sonar
EKF	extended Kalman filter
EnKF	ensemble Kalman filter
FKF	fuzzy Kalman filter
GP	Gaussian process
GP-UKF	Gaussian process-unscented Kalman filter
GPS	global positioning system
LOS	line-of-sight
NARX	non-linear autoregressive network with exogenous input
PID	photoionisation detector
RMSE	root-mean-square error
RPM	revolutions per minute
SI	system identification
UKF	unscented Kalman filter

* Contact author. Email address: wilmer.arizaramirez@utas.edu.au

1. Introduction

Development of accurate and robust navigation technologies is essential for achieving high performances in underwater environments. As the need for complex missions increases, there is a growing demand for highly accurate localisation of underwater vehicles for navigation and data collection purposes. In comparison to ground and air vehicles, localisation via the global positioning system (GPS) is rarely available under water. Therefore, navigation strategies that are more robust and independent from GPS are needed.

Strategies for navigation of underwater vehicles are to integrate the vehicle velocity from an accelerometer, gyroscope or water speed sensor to obtain a new position estimate (Dunlap and Shufeldt, 1969). If a water speed sensor is employed, the position at speeds below 0.3 m/s cannot be established, as the sensor is not capable of measuring it. In the case of inertial navigation systems, the acceleration is integrated twice with respect to time (Kuritsky and Goldstein, 1990); the double integral generates drift in the position result. This generated drift can be corrected using complementary sensors such as doppler velocity sonar (DVS), and acoustic doppler current profiler (ADCP), together with algorithms such as extended Kalman filter (EKF) and unscented Kalman filter (UKF).

In 1960, a Kalman filter was introduced as an optimal solution for state estimation from a linear system using a prediction of a physical model

(Kalman, 1960). As most systems are non-linear, the Kalman filter was modified to be used with a non-linear system by multiple techniques generating alteration as UKF and EKF. In the case of underwater vehicles, these techniques and their variations are the most popular. Armstrong et al. (2010) show that apart from the system, the EKF learn a calibration bias for the magnetic heading. However, applications that employ EKF have produced more robust and accurate results compared to the UKF (Allotta et al., 2016a; Allotta et al., 2016b; Vio et al., 2016).

Despite the positive results from UKF applications for underwater vehicles, the UKF can nevertheless demonstrate poor performance, as its predictive variances can be too small if the sigma points are not placed in the correct locations. Deficient predictive variance will produce observations with heavy weight in the measurement update, which causes the UKF to fit the noise (Turner and Rasmussen, 2010).

Other filters proposed for underwater vehicles are the ensemble Kalman filter (EnKF), fuzzy Kalman filter (FKF) and particle filter. The EnKFs represent the distribution of the system state using a random sample, called an ensemble, and replace the covariance matrix with the sample covariance computed from the ensemble (Mandel, 2009). An FKF is a combination of a fuzzy set with the Kalman filter; the fuzzy set is a mathematical technique to define inaccuracies and generate better estimation than other Kalman filters (Loebis et al., 2003).

Ngatini et al. (2017) compare the EnKF and FKF for underwater vehicles and show that the FKF exhibits better results than the EnKF. The particle filter uses a different approach to the EKF by implementing Bayesian filtering. It makes an approximation of the posterior by using a finite number of particles that represent points in the solution space. Each particle is assigned a weight, and the weighted sample points correspond to the solution of the posterior of the particle state. These particles are propagated according to the dynamics of the posterior, and the weight is modified based on support from the likelihood. The advantage of particle filters is that they do not require a state error Gaussian approximation. Despite research to increase the particle filter speeds (Telles da Silva Vale et al., 2015), the computational cost of running such algorithms is too high for an underwater vehicle's internal computers.

The principal disadvantage of these filters is that their performance depends on the accuracy of the model. The calculation of coefficients from mathematical models for underwater vehicles is a complex task that requires a series of experiments (Bishop and Parkinson, 1970), or computational fluid dynamics (CFD) simulations (Zhang et al., 2010). The quantity of data required is extended if such calculation or simulations are done within commercial vehicles, which are modular and reconfigurable. The calculation of coefficients is complex, as some coefficients are highly sensitive, and an incorrect calculation can reduce the fidelity of the predicted vehicle motion (Sen, 2000).

A solution to avoid the calculation of coefficients for a mathematical model is to use non-parametric methods. Ko et al. (2007) introduced the Gaussian process-unscented Kalman filter (GP-UKF), a modification of the standard UKF with the replacement of parametric models of state, and measurement by non-parametric models obtained from a series of experimental tests. The non-parametric models give a future state prediction and measurement, and the covariance matrices Q of process and R of measurement noises. The non-parametric model learns over a series of real experiments; it therefore includes more non-linearities than other common methods to characterise the true signal over a series of noisy samples, via the integrated smoothing function of the Gaussian process (GP).

The present paper outlines research into the capability of GP-UKF to predict and correct the measured states of an underwater vehicle. The required sample frequency and minimum training data proportion for the GP-UKF is also presented. A Simulink model of a REMUS 100 was used to produce the training data required for the non-parametric system identification and test the navigation algorithm. An ideal UKF and root-mean-square error (RMSE) were employed as comparison measures.

2. Underwater vehicle mathematical model

Fossen (1994) showed that the non-linear dynamic equations of motion of an underwater vehicle can be expressed in vector notation. This is defined by a state vector comprising the vector v of velocities on the body frame of the form $[u, v, w, p, q, r]^T$, and the vector η of position in the earth-fixed frame (Fig 1) of the form $[x, y, z, \phi, \theta, \psi]^T$, such that:

$$\mathbf{M}\dot{\mathbf{v}} + \mathbf{C}(\mathbf{v})\mathbf{v} + \mathbf{D}(\mathbf{v})\mathbf{v} + \mathbf{g}(\boldsymbol{\eta}) = \boldsymbol{\tau} \tag{1}$$

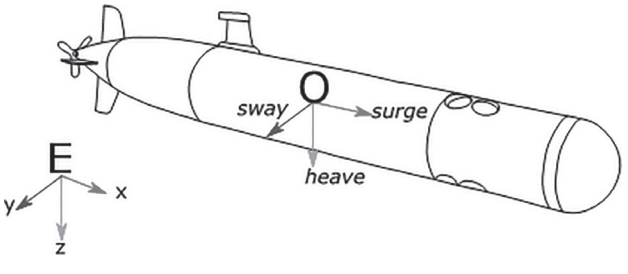

Fig 1: Underwater vehicle reference frames, vehicle frame is at centre of buoyancy

with the kinematic equation:

$$\dot{\boldsymbol{\eta}} = \mathbf{J}(\boldsymbol{\eta})\mathbf{v} \tag{2}$$

where $\boldsymbol{\eta}$ is vector of position and orientation of the vehicle in the earth-fixed frame; $\mathbf{v}$ is vector of linear and angular vehicle velocities in body fixed frame; $\dot{\mathbf{v}}$ is vector of linear and angular vehicle accelerations in body fixed frame; $\mathbf{M}$ is matrix of inertial terms; $\mathbf{C}(\mathbf{v})$ is matrix of Coriolis and centripetal terms; $\mathbf{D}(\mathbf{v})$ is matrix consisting of damping or drag terms; $\mathbf{g}(\boldsymbol{\eta})$ is vector of restoring forces and moments owing to gravity and buoyancy; $\boldsymbol{\tau}$ is vector of control and external forces; $\mathbf{J}(\boldsymbol{\eta})$ is rotation matrix that converts velocities in a body-fixed frame v to an Earth-fixed frame velocity η.

Equation 1 can be expanded into a more general equation of motion (Gertler and Hagen, 1967; Prestero, 2001). This expansion is a system of six equations with 73 hydrodynamic coefficients.

3. UKF

Table 1 shows the basic structure of the UKF that estimates the states of a dynamic system based on a series of observations and internal model. If x_k is the state of the system, u_k is the control input and z_k is the observation at time k, it can be assumed that the dynamic system evolves according to a state transition function, $f(\cdot)$, and an observation function, $h(\cdot)$, such that:

$$\begin{aligned} \mathbf{x}_k &= f\left(\mathbf{x}_{k-1}, \mathbf{u}_{k-1}\right) + \boldsymbol{\varepsilon}_k \\ \mathbf{y}_k &= h\left(\mathbf{x}_k\right) + \boldsymbol{\delta}_k \end{aligned} \tag{3}$$

where ε_k is additive with zero-mean Gaussian noise with covariance Q_k, and $\boldsymbol{\delta}_k$ is the additive observation noise with covariance $\mathbf{R}_k$. The functions $f(\cdot)$ and $h(\cdot)$ are non-linear, even when the estimate of the state $\mathbf{X}_{k-1}$ is Gaussian; the estimate after passing the states through the transition function $f(\cdot)$ is no longer Gaussian. To estimate posteriors over the state space model, the UKF requires a stochastic approximation known as the unscented transform (Uhlmann, 1995). The unscented transform works by calculating a set of sigma points that are transformed through the non-linear functions and their respective Gaussian distribution.

Table 1: UKF algorithm

$\text{UKF}\left(\hat{x}_{k-1\|k-1}, P_{k-1\|k-1}, u_{k-1}, z_k, f(\cdot), h(\cdot)\right)$
⟩Prediction
1 : $\hat{x}_{k|k-1}, P_{k|k-1} \leftarrow UT\left(\hat{x}_{k-1\|k-1}, P_{k-1\|k-1}, u_{k-1}, f(\cdot)\right)$
2 : $P_{k|k-1} \leftarrow P_{k|k-1} + Q$
⟩Correction
3 : $\hat{z}_{k|k-1}, S_k, C_k \leftarrow UT\left(\hat{x}_{k|k-1}, P_{k|k-1}, h(\cdot)\right)$
4 : $S_k \leftarrow S_k + C_k S_k^{-1}\left(z_k - \hat{z}_{k|k-1}\right)$
5 : $\hat{x}_{k|k} \leftarrow \hat{x}_{k|k-1} + C_k S_k^{-1}(z_k - \hat{z}_{k|k-1})$
6 : $P_{k|k} \leftarrow P_{k|k-1} + C_k S_k^{-1} C_k^T$
end

4. Regression with GPs

A GP is a non-parametric tool capable of learning regression functions from discrete training data. Benefits of GPs include model flexibility, and the abilities to provide uncertainty estimates and learn noise and smoothness parameters from training data (Rasmussen, 2004). A GP represents the posterior distributions over functions based on training data (Ebden, 2008). It assumes that the data is derived from a noisy process of the form:

$$y_i = f(\mathbf{x}_i) + \varepsilon \tag{4}$$

where ε is a zero-mean additive Gaussian noise with variance σ_n^2. A test input x_*, conditioned in a set of data $\langle \mathbf{x}, \mathbf{y} \rangle$ will produce a Gaussian distribution with mean:

$$y_* \left| \mathbf{X}, \mathbf{y}, x_* = \mathbf{K}(\mathbf{X}, \mathbf{X})\left[\mathbf{K}(\mathbf{X}, \mathbf{X}) + \sigma_n^2 \mathbf{I}\right]^{-1} \mathbf{y} \right. \tag{5}$$

and variance:

$$\begin{aligned} \operatorname{cov}(y_*) = k\left(x_*, x_*\right) - \mathbf{k}\left(x_*, X\right)[\mathbf{K}(\mathbf{X}, \mathbf{X}) \\ + \sigma_n^2 \mathbf{I}]^{-1} \mathbf{k}\left(X, x_*\right) \end{aligned} \tag{6}$$

where $k(x_*, x_*)$ is the evaluation of the kernel with respect to the test point x_*; $\mathbf{k}(x_*, X)$ is a vector defined by kernel values between x_* and the training inputs; $\mathbf{K}(\mathbf{X}, \mathbf{X})$ is the square kernel matrix of the training input values.

The prediction uncertainty captured by the variance depends on the process noise and the correlation between the test input and training data. The kernel function selection is governed by application; the most widely used is the squared exponential, or Gaussian kernel, which is considered a universal kernel:

$$k_{\text{SE}}(x, x') = \sigma^2 \exp\left(-\frac{(x - x')^2}{2\ell^2}\right) \tag{7}$$

where σ^2 controls the average distance of the function away from its mean. The length scale, l, determines the twist length in the function.

There are two principal methods for learning the hyperparameters Θ, which are Bayesian model interference and marginal likelihood. Bayesian inference assumes that prior data of the unknown function to be mapped is known. A posterior distribution over the function is refined by incorporation of observations. The marginal likelihood method is based on the aspect that some hyperparameters are

more noticeable in their effect over the posterior distribution. Over this base the posterior distribution of hyperparameters can be described with a unimodal, narrow Gaussian distribution (Rasmussen, 2004).

The learning of GPs' hyperparameters Θ is normally achieved by maximisation of the marginal likelihood. The marginal likelihood can be expressed as:

$$p(\mathbf{y}\,|\,\mathbf{x},\boldsymbol{\Theta}) = \frac{1}{(2\pi)^{\frac{N}{2}}\,|\mathbf{K}|^{\frac{1}{2}}}\, e^{-\frac{1}{2}\mathbf{y}^T\mathbf{K}^{-1}\mathbf{y}} \tag{8}$$

where N is the number of input learning data points and y is a vector of learning output data of the form $[y_1; y_2; \ldots y_N]$. To reduce the calculation complexity, it is preferred to use the logarithmical marginal likelihood obtained by the application of logarithmic properties to equation 8:

$$\mathrm{L}(\boldsymbol{\Theta}) = -\frac{1}{2}\log(|\mathbf{K}|) - \frac{1}{2}\mathbf{y}^T\mathbf{K}^{-1}\mathbf{y} - \frac{N}{2}\log(2\pi) \tag{9}$$

To find a solution for the maximisation of log-likelihood multiples, methods of optimisation can be applied, e.g. particle swarm optimisation, genetic algorithms or gradient descent. For deterministic optimisation methods, the computation of likelihood of partial derivatives with respect to each hyperparameter is needed. According to Williams and Rasmussen (2006), log-likelihood derivatives for each hyperparameter can be calculated by:

$$\begin{aligned}\frac{\partial \mathrm{L}(\boldsymbol{\Theta})}{\partial \boldsymbol{\Theta}_i} = &-\frac{1}{2}\mathit{trace}\left(\mathbf{K}^{-1}\frac{\partial \mathbf{K}}{\partial \boldsymbol{\Theta}_i}\right)\\ &+\frac{1}{2}\mathbf{y}^T\mathbf{K}^{-1}\frac{\partial \mathbf{K}}{\partial \boldsymbol{\Theta}_i}\mathbf{K}^{-1}\end{aligned} \tag{10}$$

5. GP-UKF

The objective of the GP-UKF is to replace the internal parametric model f used for state calculation and observation model h with a non-parametric model generated by GPs, and to use the respective variance for the calculation of $\mathbf{Q}_k$ and $\mathbf{R}_k$. The process noise covariance is obtained from the predictive GP uncertainty at the previous mean sigma point and used for the calculation of the sigma points. The sigma points are passed through the GP observation model, and the observation error covariance is obtained from the observation GP.

Table 2 shows the basic structure of the GP-UKF algorithm. The incorporation of GP regression allows GP-UKFs to learn their models and noise processes from training data. The noise models of the filter automatically adapt to the system states depending on the density of training data around the current state. Consequently, if the calculation is outside the identified region, the GP-UKF produces higher uncertainty estimates, reflecting the higher uncertainty in the underlying process model.

Table 2: GP-UKF algorithm

$$\mathrm{GP-UKF}\left(\hat{\mathrm{x}}_{k-1|k-1}, \mathrm{P}_{k-1|k-1}, \mathrm{u}_{k-1}, \mathrm{z}_k, \mathrm{GP-f}(\cdot), \mathrm{GP-h}(\cdot)\right)$$

⟩Prediction

$$\hat{\mathrm{x}}_{k|k-1}, \mathrm{P}_{k|k-1}, \mathrm{Q}_k \leftarrow UT\left(\hat{\mathrm{x}}_{k-1|k-1}, \mathrm{P}_{k-1|k-1}, \mathrm{u}_{k-1}, \mathrm{GP-f}(\cdot)\right)$$

$$\mathrm{P}_{k|k-1} \leftarrow \mathrm{P}_{k|k-1} + \mathrm{Q}_k$$

⟩Correction

$$\hat{\mathrm{z}}_{k|k-1}, \mathrm{S}_k, \mathrm{C}_k, \mathrm{R}_k \leftarrow UT\left(\hat{x}_{k|k-1}, P_{k|k-1}, \mathrm{GP}-h(\cdot)\right)$$

$$\mathrm{S}_k \leftarrow \mathrm{S}_k + \mathrm{R}_k$$

$$\hat{\mathrm{x}}_{k|k} \leftarrow \hat{\mathrm{x}}_{k|k-1} + \mathrm{C}_k\mathrm{S}_k^{-1}(\mathrm{z}_k - \hat{\mathrm{z}}_{k|k-1})$$

$$\mathrm{P}_{k|k} \leftarrow \mathrm{P}_{k|k-1} + \mathrm{C}_k\mathrm{S}_k^{-1}\mathrm{C}_k^T$$

end

6. Test set-up and results

A simulation model of a REMUS 100 (Fig 2), based on the work of Prestero (2001) and Hall and Anstee (2011), was developed in the MATLAB/Simulink software environment and employed to produce data for test and training of the GP. A block diagram of the REMUS 100 model is shown in Fig 2. A path-following controller (Xiang et al., 2017) composed of a line-of-sight (LOS) law that pursues a point $P(t)$ and three robust photoionisation detector (PID) controllers, produces the signals for revolutions per minute (RPM), elevator force and rudder force required to control the vehicle. The controllers employ the corrupted measurement to calculate the required forces. A sample frequency of 5 Hz was used to capture data, and a sub-sample of 40 % of the data was taken randomly for the training. The training data has more points at the start of the trajectory, and the quantity of points reduces over time. Fig 3 shows the selected data for training compared to the simulation data.

The virtual sensors employed were a 3-axis gyroscope, 3-axis accelerometer, compass and doppler velocity log (DVL) unit; the measurement results produce the vector $[u,v,w,p,q,r,Z,\theta,\psi,\varphi]$. Each sensor was simulated by a model comprising an additive noise source and digitalisation of the measurement through a 12-bit ADCP. A helix movement was employed to capture 800. The AUV was accelerated from an initial velocity of 0.5 m/s to 1.4 m/s. Fig 4 shows the recorded command signals for 800 s. The noise in the depth sensor required a hard response by the integral parts of the PID, causing the vehicle to converge onto the desired path. A total of 20 simulations were carried out to

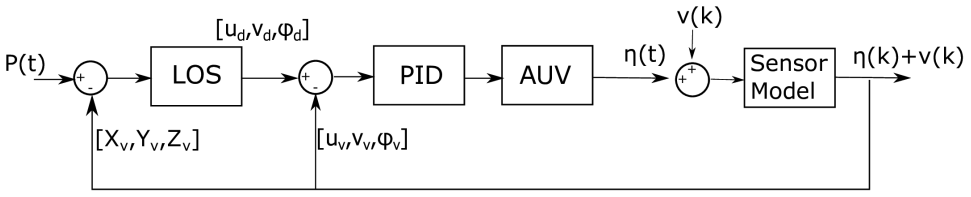

Fig 2: REMUS 100 simulation model; X_v, Y_v, Z_v are the vehicle position

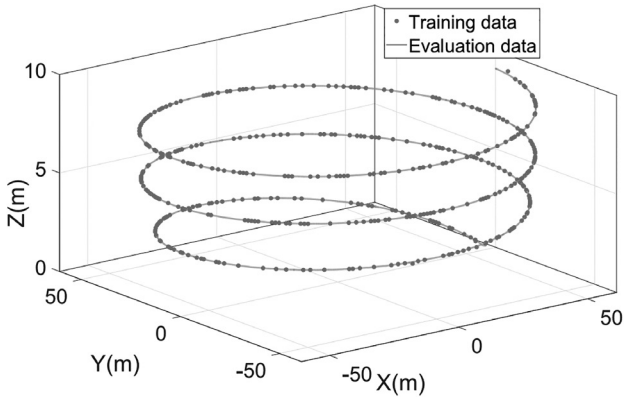

Fig 3: Training and evaluation data

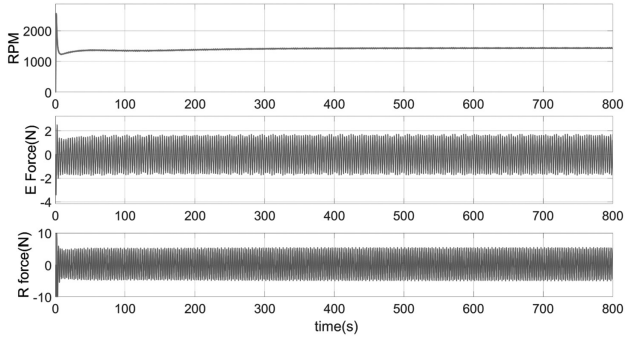

Fig 4: Helix test input signals to control surfaces

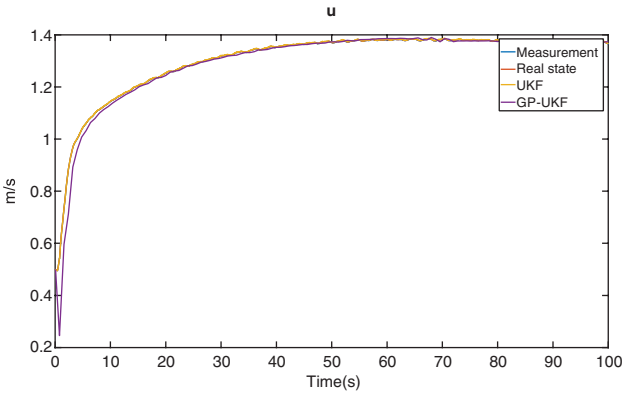

Fig 5: Surge speed comparison between corrupted measure data, real position, UKF and GP-UKF

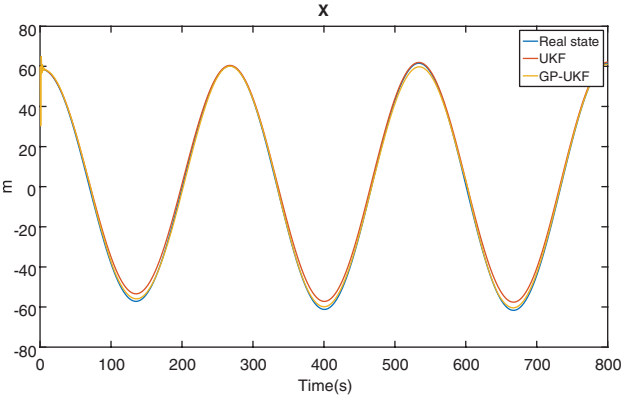

Fig 6: Predicted position state *x* comparison between UKF and GP-UKF

capture data. The first set of data was employed for the creation of the non-parametric GP model.

The state vector was defined as the combination of vehicle speeds and vehicle position $\eta = [u,v,w,p,q,r,X,Y,Z,\theta,\psi,\varphi]$. A UKF was also implemented as an evaluation measure; the filter uses the original REMUS 100 model from which the data was captured to allow comparison of the GP-UKF to an ideal UKF when all parameters from the vehicle are known. The GP-UKF and UKF were required to estimate the x and y states from the vehicle. The algorithms of Deisenroth et al. (2009) were employed with minor modification to the GP to allow a non-linear autoregressive network with exogenous input (NARX) structure to be utilised for system identification (SI). The modification included the assembly of the input vector for learning as $Xd = [\eta, ui]$, where η is the state vector and ui is the command signal. The output vector is formed from the delay vector $Y\,d = Xd(k-1, k-2)$.

Fig 5 shows the comparison between the measured data of the real vehicle state, UKF and GP-UKF. The GP-UKF is equally capable of correcting the measurement state of the vehicle, as the positioning of the sigma points is estimated from the GP's dynamic model. The predicted position states (Figs 6 and 7) from the GP-UKF x and y have a higher similarity to the vehicle's real position; although the GP employs data corrupted by noise, it has learned to predict over this data.

The comparison of the vehicle position estimations and real position is shown in Fig 8. The UKF shows a drift in the calculation of x and y over time. In comparison to the UKF, the GP-UKF demonstrates better performance in the prediction of the vehicle position for both the horizon of the training data from the GP, and the decay outside the

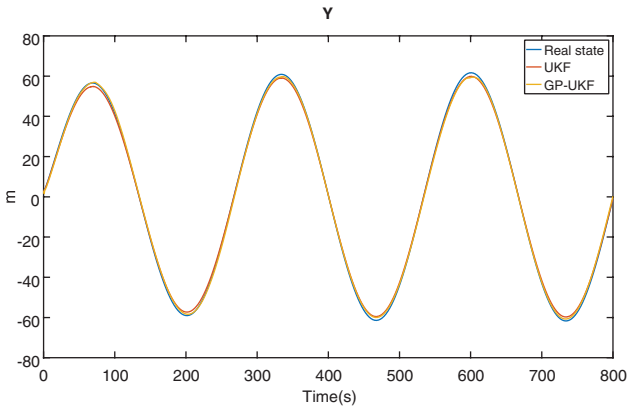

Fig 7: Predicted position state *y* comparison between UKF and GP-UKF

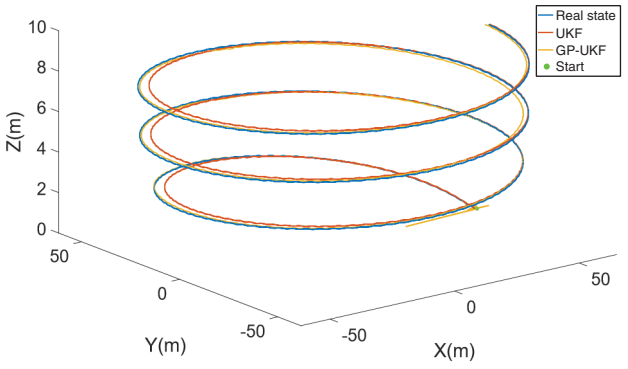

Fig 8: Comparison of position estimation between real state, UKF and GP-UKF

Table 3: Mean RMSE and standard deviation results from UKF and GP-UKF per state for 20 runs

	u(m/s)	v(m/s)	w(m/s)	p(rad/s)	q(rad/s)	r(rad/s)
UKF	0.0014	0.0015	0.0005	0.0023	0.0013	0.0031
σ-UKF	0.0003	0.0021	0.0008	0.0078	0.0035	0.0121
GP-UKF	0.0158	0.0369	0.0154	0.0569	0.0601	0,1813
σ-GP-UKF	0.0387	0.0069	0.0033	0.0123	0.0130	0,0347
	X(m)	**Y(m)**	**Z(m)**	**ϕ(rad)**	**θ(rad)**	**ψ(rad)**
UKF	2.4237	1.2695	0.0017	0.0006	0.0012	0.0013
σ-UKF	14.6908	8.5834	0.0019	0.0020	0.0016	0.0988
GP-UKF	2.0541	1.3894	0.0281	0.0235	0.0297	0.1095
σ-GP-UKF	11.1893	9.9445	0.1889	0.0047	0.0052	0.3848

Table 4: Mean RMSE results from UKF and GP-UKF for correction and prediction

RMSE	Value
RMSE-UKF correction	0.0028
RMSE-GP-UKF correction	0.086
RMSE-UKF prediction	2.91
RMSE-GP-UKF prediction	2.86

training horizon. Although the error increases outside the training horizon, this is corrected by the filter in the return to the training horizon.

Tables 3 and 4 summarise the measurement of the mean RMSE between the real vehicle states and the correction from the UKF and the GP-UKF for the 20 simulations. The results confirm that the GP-UKF can perform as reliably as an ideal UKF, and in some cases it can overperform the ideal UKF. Table 4 shows the average measurement for correction and prediction. In the case of prediction, the GP-UKF can forecast vehicle position with higher precision than an ideal UKF, as the inclusion of the noise function and smooth prediction of the GP supports the ability of the UKF to predict position.

7. Conclusion

The present research demonstrates that the GP-UKF is a promising approach for state estimation in applications where accurate parametric model is not available. The GP-UKF shows similar performance compared to an ideal UKF in the prediction and correction of the vehicle states for the helix movement test case. The average RMSE (as shown in Table 4) for prediction and correction shows that non-parametric models can be employed as prediction models inside the Kalman filter as the UKF for autonomous underwater vehicles (AUVs).

The GP-UKF demonstrates better performance in the prediction of states than the UKF. The smoothing kernel of the GP facilitated a smooth transition between the prediction points and better placement of sigma points. The tuning complexity in the implementation of a non-linear Kalman filter is reduced dramatically, as the user is not required to produce the covariance matrices for the process and measure noise model. The GP-UKF can be converted to an important tool for underwater vehicles, especially in cases where high non-linearities are expected, such as in operations near surface or near another object, or during specialised missions. Another advantage of GP-UKF is that it can be used even when no GPS signal is available, which is essential for correction in traditional Kalman filters. An underwater vehicle can switch between filters as the availability of data is reduced.

The principal disadvantage of GP models is their computational cost during training. Nonetheless, research has shown that this cost can be reduced by using sparse GP models, thus allowing the use of

more complex models or configurations. Further work is currently ongoing to prepare an AUV for a series of experiments to train its GP-based, non-parametric model. Once trained and verified, the vehicle will be deployed to assess the performance of the GP-UKF outside a controlled environment.

References

Allotta B, Caiti A, Chisci L, Costanzi R, Di Corato F, Fantacci C, Fenucci D, Meli E and Ridolfi A. (2016a). An unscented Kalman filter based navigation algorithm for autonomous underwater vehicles. *Mechatronics* **39**: 185–195.

Allotta B, Caiti A, Costanzi R, Fanelli F, Fenucci D, Meli E and Ridolfi A. (2016b). A new AUV navigation system exploiting unscented Kalman filter. *Ocean Engineering* **113**: 121–132.

Armstrong B, Wolbrecht E and Edwards DB. (2010). AUV navigation in the presence of a magnetic disturbance with an extended Kalman filter. In: Proceedings of IEEE Oceans 2010 Sydney, 24–27 May, Sydney, Australia.

Bishop RED and Parkinson AG. (1970). On the planar motion mechanism used in ship model testing. *Philosophical Transactions of the Royal Society of London* **266***:* 35–61.

Deisenroth MP, Huber MF and Hanebeck UD. (2009). Analytic moment-based gaussian process filtering. In: Bottou L and Littman M. (eds.) *Proceedings of the ICML 2009 26th Annual International Conference on Machine Learning*, 14–18 June, Montreal, Quebec, Canada, 225–232.

Dunlap G and Shufeldt HH. (1969). *Dutton's navigation and piloting*, 12th edition. Annapolis, Maryland: Naval Institute Press, 715pp.

Ebden M. (2008). Gaussian processes for regression: a quick introduction. Robotics Research Group, Department of Engineering Science, University of Oxford. Available at <https://arxiv.org/pdf/1505.02965.pdf, last accessed 1 June 2019>.

Fossen TI. (1994). *Guidance and control of ocean vehicles*. New York: Wiley, 480pp.

Gertler M and Hagen GR. (1967). *Standard equations of motion for submarine simulation.* Bethesda, Maryland: David W Taylor Naval Ship Research and Development Center. Available at <https://apps.dtic.mil/dtic/tr/fulltext/u2/653861.pdf, last accessed 1 June 2019>.

Hall R and Anstee S. (2011). *Trim calculation methods for a dynamical model of the REMUS 100 autonomous underwater vehicle*. Australian Government Department of Defence, Maritime Operations Division, Defence Science and Technology Organisation, DSTO-TR-2576. Available at <https://apps.dtic.mil/dtic/tr/fulltext/u2/a554483.pdf, last accessed 1 June 2019>.

Kalman RE. (1960). A new approach to linear filtering and prediction problems. *ASME–Journal of Basic Engineering* **82**: 35–45.

Ko J, Kleint DJ, Fox D and Haehnel D. (2007). GP-UKF: Unscented Kalman filters with Gaussian process prediction and observation models. In: Proceedings of the 2007 IEEE/RSJ International Conference on Intelligent Robots and Systems, 29 October–2 November, San Diego, California, USA.

Kuritsky MM and Goldstein MS. (1990). Inertial navigation. In: Cox IJ and Wilfong GT. (eds.) *Autonomous robot vehicles*. New York: Springer-Verlag, 96–116.

Loebis D, Sutton R and Chudley J. (2003). A fuzzy Kalman filter for accurate navigation of an autonomous underwater vehicle. In: (eds.) Roberts GN, Sutton R and Allen R. *Proceedings of the IFAC Workshop on Guidance and Control of Underwater Vehicles 2003*. 9–11 April 2003, Newport, South Wales, UK **36**: 157–162.

Mandel J. (2009). A brief tutorial on the ensemble Kalman filter. Available at <https://arxiv.org/abs/0901.3725, last accessed 1 June 2019>.

Ngatini T, Apriliani E and Nurhadi H. (2017). Ensemble and fuzzy Kalman filter for position estimation of an autonomous underwater vehicle based on dynamical system of AUV motion. *Expert Systems with Applications* **68**: 29–35.

Prestero T. (2001). *Verification of a six-degree of freedom simulation model for the REMUS autonomous underwater vehicle*. BS thesis, University of California at Davis, Davis, California, USA. Available at <https://core.ac.uk/download/pdf/4429735.pdf, last accessed 1 June 2019>.

Rasmussen CE. (2004). Gaussian processes in machine learning. In: Bousquet O, von Luxburg U and Rätsch G. (eds.) *Advanced lectures on machine learning*. Berlin: Springer-Verlag, 63–71.

Sen D. (2000). A study on sensitivity of manoeuvrability performance on the hydrodynamic coefficients for submerged bodies. *Journal of Ship Research* **45**: 186–196.

Telles da Silva Vale R, Apolonio de Barros E and de Castro Martins T. (2015). GPU-accelerated Monte Carlo localization for underwater robots. *IFAC-PapersOnLine* **48**: 76–81.

Turner R and Rasmusbluesen CE. (2010). Model based learning of sigma points in unscented Kalman filtering. In: Kaski S, Miller DJ, Oja E and Honkela A. (eds.) *Proceedings of the 2010 IEEE International Workshop on Machine Learning for Signal Processing (MLSP 2010)*. 29 August–1 September 1, Kittilä, Finland, 178–183.

Uhlmann JK. (1995). *Dynamic map building and localization: new theoretical foundations*. PhD thesis, University of Oxford, Oxford, UK. Available at <http://faculty.missouri.edu/uhlmannj/Dissertation-pref.pdf, last accessed 1 June 2019>.

Vio RP, Cristi R and Smith KB. (2016). Near real-time improved uuv positioning through channel estimation – the unscented Kalman filter approach. In: Proceedings of MTS/IEEE Oceans 2016 Monterey, 19–23 September, Monterey, California, USA.

Williams CKI and Rasmussen CE. (2006). *Gaussian processes for machine learning*. Cambridge: The MIT Press, 248pp.

Xiang X, Yu C and Zhang Q. (2017). Robust fuzzy 3D path following for autonomous underwater vehicle subject to uncertainties. *Computers & Operations Research* **84**: 165–177.

Zhang H, Xu Y. and Cai H. (2010). Using CFD software to calculate hydrodynamic coefficients. *Journal of Marine Science and Application* **9**: 149–155.